Scanning tunneling microscopy. I. Theoretical framework and coherence effects

V. M. Kenkre
Department of Physics and Astronomy, University of New Mexico, Albuquerque, New Mexico 87131

F. Biscarini* and C. Bustamante
Department of Chemistry and Institute of Molecular Biology, University of Oregon, Eugene, Oregon 97403
(Received 22 July 1994)

A theoretical formalism for the interpretation of scanning-tunneling-microscopy (STM) images is developed with special attention to the effects of adsorbate molecules placed in the tip-substrate gap. The STM configuration is treated as a system of three groups of states, the substrate, the adsorbate, and the tip, in contact with a thermal reservoir, with which it exchanges energy as well as particles. The calculation of the observed current is approached as a transport problem in quantum statistical mechanics with focus on the description of the arbitrary degree of quantum coherence in the tunnel junction and of the temperature and complexity of the adsorbate. Expressions are obtained for the STM current and for the effective resistance of the STM junction. They are shown to allow one to relax some of the restrictive assumptions made in existing approaches. Particular cases are worked out, observable quantum interference effects are predicted, and simple examples suggesting the nature of the mechanism of contrast of adsorbed molecules are presented along with the corresponding images.

I. INTRODUCTION

The purpose of this paper is to formulate a theoretical framework for the interpretation of images of adsorbates in scanning tunneling microscopy (STM). Since its invention,[1] STM has been employed to produce high-resolution images of bare conductive surfaces as well as of atoms and molecules adsorbed on conductive substrates. While data have appeared in abundance, some crucial questions of interpretation have remained open. Important examples of features that have not been understood completely are the nature of the giant corrugation observed in STM images of low-indices metal surfaces,[2,3] the nature of contrast in images of organic molecules on conductive substrates,[4,5] and the limit of resolution in molecular adsorbates.[6] Other examples include dissipative effects in the STM junction and the temperature dependence of the tunneling current. Indeed, there is a definite lack of a straightforward set of prescriptions that the experimentalist could use to assign a feature in an observed STM image to a specific factor and theoretical methods are important tools in understanding the microscopic origin of contrast in STM images.

The primary task of STM theories, viz., the calculation of the tunneling current in terms of the microscopic variables representing the STM junction, is complicated by the fact that the STM junction is a mesoscopic system with a large number of degrees of freedom, that few symmetries exist in the STM configuration to ease the calculational problem, that the tip structure is unknown, and that local motion of the atoms involved, as well as the mechanical instabilities of the tunneling gap, can affect the transmission of electrons across the junction. A number of simple one-dimensional tunneling barrier models[7–9] have been developed to address the resolution of STM experiments. The necessity of explaining nontopographical features in STM images has prompted more realistic and detailed theories capable of addressing the three-dimensional atomic nature of the STM junction.[10–13] The main focus in these theories has been on the relationship between the STM current and equilibrium electronic-structure properties such as the local density of states, the tip electronic structure, the focusing of the current due to the tip apex atom, the changes in the space distribution of the STM current in the presence of adatoms, and the importance of interference effects in limiting the resolution of molecular adsorbates.

Well-known and successful examples of existing approaches[10,14] include the Tersoff-Hamann theory[10] based on the transfer Hamiltonian method,[15] which uses time-dependent perturbation theory. The key result is a simple and convenient relation between the tunneling current and the substrate local density of states at the Fermi level, evaluated at the tip position. The relation is a powerful feature of the theory and has led to the simulation of STM images of metal and semiconductor surfaces[16–18] in agreement with experimental results. Lang's theory[14] has succeeded in showing that, at low bias voltage, the relation between current and local density of states at the Fermi level holds also for adatoms. Several authors have expressed the opinion, however, that the underlying perturbative approach to the STM current may not be adequate in all experimental situations and have proposed current definitions that are claimed to go beyond the perturbative regime. Implicit assumptions in perturbative treatments are that the tip-substrate interaction is weak, that the temperature is not high enough to complicate simple quantum-mechanical transfer among sharp levels, and that incoherence in the transfer is large enough to validate the use of the Fermi golden rule. Thus it has been pointed out by Chen[19] and by Sacks and Noguera[20] that, in order to answer the problem of the giant corruga-

0163-1829/95/51(16)/11074(16)/$06.00

©1995 The American Physical Society

tion in metal surfaces, it is necessary to relax some of the assumptions implicit in a perturbative approach and redefine the STM current on the basis of more general arguments. The contact resistance experiment by Gimgewski and Möller[21] has brought up the necessity of nonperturbative theories of current in the context of the observed current-separation characteristics. Work towards this particular end has been performed by Lang,[22] Tsukada *et al.*,[23] Doyen *et al.*,[24] Noguera,[25] and Chen[26] and has consisted of the extension of the transfer Hamiltonian tunneling current using the wave function of the combined system tip sample. Sautet and Joachim[27] have adopted the scattering matrix approach and the generalization of Landauer's theory of current to three-dimensional transport to calculate the tunneling current through molecular adsorbates. Except for Tsukada and Shima's work,[12] which studies the tunneling of an electron dressed with surface phonons, none of the other methods has taken into explicit account the effect of the bath interactions on the tunneling current. The molecular-dynamics simulation of a metal-tip–metal-substrate system by Todorov and Sutton,[28] along with a calculation of the current with the theory by Pendry, Prêtre, and Kreutzer,[29] represents another attempt to treat electronic and (indirectly) thermal effects on the STM current.

It should be clear from the above discussion that it is important, and timely, to forge a comprehensive theoretical tool for the interpretation of STM images. In the present paper, we develop a framework that is capable of treating some of the issues discussed above. One of the features we concentrate on is the effect of arbitrary degree of coherence of electron transfer across the junction:[30] this degree of coherence is determined by the relative strengths of the interatomic matrix elements and bath interactions. A study of such coherence effects has long been important and useful in other transfer situations as in exciton dynamics.[31,32] In the STM context, local disorder, relaxation of the interface, and mechanical and thermal instabilities would lead to the incoherent regime, while close tip-substrate separations (2–3 Å), formation of localized bonds, chemisorption at the electrodes, and strong fields would favor a coherent regime. Since all these factors are usually present during an actual STM experiment, it is likely that electron motion in a STM junction would possess character intermediate between the two limit regimes. A theoretical interpretation scheme capable of treating *such intermediate coherence* is thus an important undertaking and is one of the points of emphasis of our theory.

The paper is set out as follows. In Sec. II we describe our approach and state the primary results of our theory, which consist of expressions for the effective resistance of the STM junction and for the STM current. In Sec. III we show the details of the derivation of the results. In Sec. IV we work out several simple but useful examples from our theory. These examples address, among other issues, that of coherence of electron transfer and involve predictions including a resistance minimum that arises from quantum interference. In Sec. V we present simple STM images for illustrative systems and discuss aspects of lateral resolution and energy mismatch in STM. Finally, in Sec. VI we present a summary and discussion.

II. OUR APPROACH AND STATEMENT OF THE PRIMARY RESULTS

We look upon the STM junction as a system consisting of three parts: the substrate (labeled S), the tip (T), and the adsorbed molecular entity (M). We begin with each of these parts represented by a single quantum-mechanical state, derive essential results, and then generalize to the actual situations in which each part consists of a multitude of states. The states in the three corresponding groups will be labeled by σ, τ, and μ in the generalization. In the interest of greater applicability, we abandon commitment to any particular transport equation for the electrons at the outset and develop the theory generally in terms of electron propagators. We develop expressions for the current in terms of these (probability) propagators and only later on in the development calculate the propagators and study the effects explicitly.

Our three primary results are an expression for the effective resistance of the STM junction in terms of its microscopic properties, a prescription for the calculation of the steady-state STM current, and an expression for the transient STM current. The first two are applicable immediately to existing observations, while the third would be of interest to future time-resolved STM experiments.

Our expression for the effective resistance $R_{\rm eff}$ is

$$R_{\rm eff}=\frac{1}{e^2 n_e}\left\{\frac{\int_0^{+\infty}dt[\Pi_{SS}(t)-\Pi_{ST}(t)]}{\left[\frac{\Delta\eta_S^{\rm th}}{\mu-\mu_S}\right]}+\frac{\int_0^{+\infty}dt[\Pi_{TT}(t)-\Pi_{TS}(t)]}{\left[\frac{\Delta\eta_T^{\rm th}}{\mu-\mu_T}\right]}\right\}. \quad (2.1)$$

Here e is the electron charge magnitude, n_e is the number of electrons in the STM junction, μ is the equilibrium chemical potential of the system, and μ_T and μ_S are the chemical potentials imposed by the driving reservoirs on the tip and the substrate, respectively. The difference $\mu_S-\mu_T$ is proportional to the bias voltage ϕ_{TS} at the tip. The quantity $\Delta\eta^{\rm th}$ is the difference in the equilibrium population originating from the local variation of the chemical potential with respect to the equilibrium potential that arises from the presence of driving reservoirs. Specifically, $\Delta\eta_T^{\rm th}=\eta_T^{\rm th}-P_T^{\rm th}$, where $\eta_T^{\rm th}$ is the electron probability at the tip in the absence of a driving agency and $P_T^{\rm th}$ is the quasiequilibrium population imposed by the reservoir in contact with the tip. The Π's are averages of propagators that describe the motion of the electron in the absence of driving reservoirs: $\Pi_{mn}(t)$ is the probability to find the electron at time t in the state m given that it was placed in the state n at the initial time. The labels T and S denote appropriate averages over groups of states representative of the tip and the substrate, respectively.

Our prescription for the calculation of the steady-state STM current I is

$$I=\frac{en_e}{2}\left\{\frac{\Delta\eta_T^{\rm th}}{\int_0^{+\infty}dt[\Pi_{TT}(t)-\Pi_{TS}(t)]}-\frac{\Delta\eta_S^{\rm th}}{\int_0^{+\infty}dt[\Pi_{SS}(t)-\Pi_{ST}(t)]}\right\}. \tag{2.2}$$

Our expression for the time-dependent STM transient current is

$$I=\frac{en_e}{2}\left\{\int_0^t ds[\lambda_T(t-s)\eta_T(s)-\lambda_S(t-s)\eta_S(s)]-P_T^{\rm th}\int_0^t ds\,\lambda_T(s)+P_S^{\rm th}\int_0^t ds\,\lambda_T(s)\right\}, \tag{2.3a}$$

where the response functions $\lambda_T(t)$ and $\lambda_S(t)$ are defined as

$$\int_0^{+\infty}dt\,\lambda_T(t)e^{-\varepsilon t}=\frac{1}{\int_0^{+\infty}dt[\Pi_{TT}(t)-\Pi_{TS}(t)]e^{-\varepsilon t}},$$
$$\int_0^{+\infty}dt\,\lambda_S(t)e^{-\varepsilon t}=\frac{1}{\int_0^{+\infty}dt[\Pi_{SS}(t)-\Pi_{ST}(t)]e^{-\varepsilon t}}, \tag{2.3b}$$

where ε is the Laplace variable.

Further important simplified results arising from (2.1) and (2.2) are respective expressions for the low-temperature, low-voltage, and low-temperature–low-voltage regimes. At temperatures low with respect to the Fermi temperature, the expression for the effective resistance is (2.1) with the replacement of μ by the Fermi energy E_F. In the low-voltage limit, the effective resistance becomes independent of the applied voltage:

$$R_{\rm Ohm}=\lim_{\phi_{TS}/k_B\theta\to 0}\frac{\phi_{TS}}{I}=\frac{1}{e^2}\left[\frac{\int_0^{+\infty}dt[\Pi_{TT}(t)-\Pi_{TS}(t)]}{\left[\frac{\partial n_T}{\partial\mu}\right]_\theta}+\frac{\int_0^{+\infty}dt[\Pi_{SS}(t)-\Pi_{ST}(t)]}{\left[\frac{\partial n_S}{\partial\mu}\right]_\theta}\right], \tag{2.4}$$

where $n_S=n_e\eta_S^{\rm th}$ and $n_T=n_e\eta_T^{\rm th}$ denote, respectively, the number of electrons at the substrate and the tip, θ is the absolute temperature, and the isothermal partial derivative of the electron number with respect to the chemical potential is inversely proportional to $k_B\theta$ at high temperature, as is obvious from the statistical mechanics of the grand canonical ensemble. The further limit of low temperatures reduces this Ohmic resistance $R_{\rm Ohm}$ to

$$\lim_{k_B\theta/E_F\to 0}R_{\rm Ohm}=\frac{1}{e^2}\left\{\frac{1}{G_T^0}\int_0^{+\infty}dt[\Pi_{TT}(t)-\Pi_{TS}(t)]+\frac{1}{G_S^0}\int_0^{+\infty}dt[\Pi_{SS}(t)-\Pi_{ST}(t)]\right\}, \tag{2.5}$$

where G_T^0 and G_S^0 are the projected densities of states at the tip and substrate, respectively, evaluated at the Fermi energy E_F.

III. DERIVATION OF OUR RESULTS

We begin with a simplified STM junction consisting of just a single tip state T, a single substrate state S, and an arbitrary number of states of the absorbed molecule and later on generalize the analysis to arbitrary number of states in the tip and the substrate.[33]

A. Simplified analysis

We do not specify the detail of the nature of motion, which could be coherent or incoherent, bath affected, or otherwise, and develop the theory in terms of the electron probability propagators mentioned in Sec. II above. In the absence of a driving agency, the probability $\eta_m(t)$ that the electron occupies the state $|m\rangle$ (S, T, or the adsorbed molecule states) at time t will be given in terms of the propagators $\Pi(t)$ and the initial conditions $P(0)$ as

$$\eta_m(t)=\sum_n\Pi_{mn}(t)P_n(0). \tag{3.1}$$

Consider now that a driving agency consisting of particle reservoirs connected to the tip and the substrate forces a current through the junction by causing removal of the electron from the tip state $|T\rangle$ at rate $R_T(t)$ with accompanying reentrance at the substrate state at rate $R_S(t)$. The equation of motion in the driven system is thus

$$\frac{dP_m(t)}{dt}=(\text{gain-loss})_m-\delta_{m,T}R_T(t)+\delta_{m,S}R_S(t), \tag{3.2}$$

where the gain-loss term represents changes in population due to interactions within the system. We have refrained from writing explicit forms for the gain-loss term to emphasize that the results we derive are independent of their specific form and to allow us to use a variety of transport equations of motion depending on the system.

The current at the tip is given by $I(t)=en_eR_T(t)$, where n_e is the number of electrons involved. If we invoke the fact that no charge accumulation occurs within the STM junction in the course of an experiment, ignoring thus extremely short time effects, we can equate the tip current to the substrate current and also write $I(t)=en_eR_S(t)$, since, from probability conservation, $R_T(t)$ and $R_S(t)$ will be equal to each other. The linearity of the equations of motion, whatever their detailed content, results in

$$P_m(t)=\eta_m(t) + \left[\int_0^t dt' R_T(t')[\Pi_{mS}(t-t')-\Pi_{mT}(t-t')]\right] , \tag{3.3}$$

where m can be any state: the substrate S, the tip T, or the molecule M.

The integral equation (3.3) is formally solved for the R's in terms of Laplace transforms. If tildes denote Laplace transforms and ε is the Laplace variable, (3.3) and the corresponding equation involving R_S yield

$$\begin{aligned}\tilde{R}_T(\varepsilon)&=[\tilde{\eta}_T(\varepsilon)-\tilde{P}_T(\varepsilon)][\tilde{\Pi}_{TT}(\varepsilon)-\tilde{\Pi}_{TS}(\varepsilon)]^{-1}\\ &=\tilde{R}_S(\varepsilon)=-[\tilde{\eta}_S(\varepsilon)-\tilde{P}_S(\varepsilon)]\\ &\quad\times[\tilde{\Pi}_{SS}(\varepsilon)-\tilde{\Pi}_{ST}(\varepsilon)]^{-1} .\end{aligned} \tag{3.4}$$

The current may thus be written in the Laplace domain by

$$\tilde{I}(\varepsilon)=\frac{en_e}{2}\left\{\frac{\tilde{\eta}_T(\varepsilon)-\tilde{P}_T(\varepsilon)}{\tilde{\Pi}_{TT}(\varepsilon)-\tilde{\Pi}_{TS}(\varepsilon)}+\frac{\tilde{P}_S(\varepsilon)-\tilde{\eta}_S(\varepsilon)}{\tilde{\Pi}_{SS}(\varepsilon)-\tilde{\Pi}_{ST}(\varepsilon)}\right\} , \tag{3.5}$$

in terms of the propagators Π, the thermal populations η in the absence of the driving agency, and the actual probabilities P_t and P_S at the tip and the substrate, respectively. Until the latter two are known independently, (3.5) is no more than a formal solution.

Consider now that the entire STM junction is maintained in equilibrium with a single reservoir characterized by temperature θ and electrochemical potential μ_T. The equilibrium population at the tip will be, in standard notation,

$$P_T^{\rm th}=\sum_\xi |\langle T|\xi\rangle|^2\frac{1}{1+e^{(E_\xi-\mu_T)/k_B\theta}} , \tag{3.6}$$

where ξ denotes the *eigenstates* of the tip-molecule-substrate system. On the other hand, if the single reservoir has electrochemical potential μ_S rather than μ_T, the equilibrium population established at the substrate will be given by

$$P_S^{\rm th}=\sum_\xi |\langle S|\xi\rangle|^2\frac{1}{1+e^{(E_\xi-\mu_S)/k_B\theta}} . \tag{3.7}$$

The application of a bias voltage ϕ_{TS} means that the reservoirs in contact with the tip and the substrate are maintained at *different* electrochemical potentials μ_T and μ_S, respectively. The reservoir in contact with the tip attempts to drive the population of the tip state to the value in (3.6), whereas the reservoir in contact with the substrate attempts to make the substrate state population have the value given by (3.7). In the absence of a driving agency, μ_T and μ_S would equalize throughout the STM junction. Under the reasonable substitution of the respective values (3.6) and (3.7) for the tip and substrate probabilities in (3.5), we obtain our current expression given in Sec. II, viz., Eq. (2.2).

In order to understand precisely what dynamic details go into (2.2), we may model the sink and source terms $R_T(t)$ and $R_S(t)$ explicitly by writing (3.2) in the form

$$\frac{dP_m(t)}{dt}=(\text{gain-loss})_m-\delta_{m,T}\frac{P_T(t)-P_T^{\rm th}}{\tau_T} +\delta_{m,S}\frac{P_S^{\rm th}-P_S(t)}{\tau_S} , \tag{3.8}$$

which shows the action of the two reservoirs as driving the populations to $P_T^{\rm th}$ and $P_S^{\rm th}$, respectively, the τ's being the respective time constants. With the conservation condition $R_T(t)=R_S(t)$ employed above, (3.8) can be solved exactly to obtain the current from the relation

$$I(t)=en_e\frac{P_T(t)-P_T^{\rm th}}{\tau_T}=-en_e\frac{P_S(t)-P_S^{\rm th}}{\tau_S} . \tag{3.9}$$

In the Laplace domain, the result is

$$\begin{aligned}\tilde{I}(\varepsilon)&=en_e\frac{\tilde{\eta}_T(\varepsilon)-\dfrac{P_T^{\rm th}}{\varepsilon}}{\tau_T+[\tilde{\Pi}_{TT}(\varepsilon)-\tilde{\Pi}_{TS}(\varepsilon)]}\\ &=-en_e\frac{\tilde{\eta}_S(\varepsilon)-\dfrac{P_S^{\rm th}}{\varepsilon}}{\tau_S+[\tilde{\Pi}_{SS}(\varepsilon)-\tilde{\Pi}_{ST}(\varepsilon)]} .\end{aligned} \tag{3.10}$$

Equation (2.3) for the time-resolved current follows from (3.10) in the limit that the τ's, which are the times characteristic of the tip-reservoir and substrate interfaces, may be neglected. In order to probe properties of the STM junction most conveniently, one attempts to make these times negligible with respect to other junction characteristic times. In the following, we will assume, for simplicity, that this situation prevails and neglect the τ's. It is a trivial matter to replace it in situations in which such a neglect is not valid. In a conventional STM experiment, the acquisition time of the instrument per scanned point is of the order of 10^{-3}–10^{-6} s. As other authors[10] have pointed out, this time scale is sufficiently large for most relaxation processes to reach the steady-state regime. Consequently, it is natural to take the steady-state current I as the primary observable measured in STM experiments. Using an Abelian theorem of Laplace transforms, we multiply (3.10) by the Laplace variable ε and take the limit that ε tends to zero to obtain the steady-state result. On invoking the symmetry in (3.10) we obtain our central current expressions (2.2) and (2.3).

It is of interest to recognize that the voltage drop between the reservoirs corresponds to the bias voltage $\mu_S-\mu_T=e\phi_{TS}$ and to define the effective resistance through

$$R_{\rm eff}=\frac{(\mu_S-\mu_T)}{eI} . \tag{3.11}$$

The general expression (2.1) for the effective resistance follows from (3.11) and (2.2). If the tip and substrate have equal density of states, the electrochemical potential difference can be cast in the form

$$\mu_S-\mu_T=\left[\frac{\partial\mu}{\partial n_e}\right]_T n_e(P_S^\infty-\eta_S^{\rm th}-P_T^\infty+\eta_T^{\rm th}) , \tag{3.12}$$

where the populations P^{∞} are steady-state populations in the open system and the displacement P^{∞}-$\eta^{\rm th}$ from the equilibrium population originates from the local variation of the chemical potential with respect to the equilibrium potential. The isothermal partial derivative of the chemical potential with respect to the electron number in the classical limit is equal to $k_B\theta$, while in the quantum limit it is inversely proportional to the density of states at the Fermi level. The displacements from the equilibrium populations in (3.12) are readily calculated and the effective resistance obtained as

$$R_{\rm eff}=\frac{1}{e^2}\left[\frac{\partial\mu}{\partial n_e}\right]_\theta\int_0^{+\infty}dt\{[\Pi_{TT}(t)+\Pi_{SS}(t)]-[\Pi_{ST}(t)+\Pi_{TS}(t)]\}\ . \quad (3.13)$$

Equation (3.13) shows that the effective resistance decreases with an increase in the density of states at the Fermi level in the quantum limit (or with a decrease of the temperature θ in the classical limit) and that the form of the propagator integrals determines the spatial variation of the effective resistance. Observe that, even if the state $|M\rangle$ does not appear explicitly in the expression of the STM resistance, the existence of a state in the junction not coupled to the reservoirs but coupled to the states T and S affects the propagators. For instance, $|M\rangle$ could represent a molecular orbital from an adsorbate, an impurity, or a water molecule between tip and substrate in an STM experiment performed in a liquid or, alternatively, a localized state on the surface, a dangling bond, or the state of an adatom at the tip apex.

The expressions we have obtained for the STM current and for the effective resistance retain their validity if, instead of a single state $|M\rangle$, we take a multitude of states $\{|M\rangle\}$ not coupled to the reservoirs, as, for instance, in a cluster representation of the STM junction, provided that it is reasonable to treat the exchange of particles with the reservoirs as occurring through a single state at the tip and a single state at the substrate. The single-tip–substrate-state derivation is exact and clarifies the primary features of our approach, but has the shortcoming that, being based on a single-state representation of the tip and the substrate, it describes only a highly idealized system. In a realistic case we must take into account the large number of states involved at the tip and the substrate. A generalization of our approach for this purpose may be carried out as follows.

B. Generalized analysis

In order to carry out a generalization of the formulation presented in the preceding subsection, we denote the individual tip and substrate states by τ and σ, respectively, and replace (3.6)–(3.9) by

$$P_T^{\rm th}=\frac{1}{n_e}\sum_\tau\sum_\xi|\langle\tau|\xi\rangle|^2\frac{1}{1+e^{(E_\xi-\mu_T)/k_B\theta}}\ ,$$
$$P_S^{\rm th}=\frac{1}{n_e}\sum_\sigma\sum_\xi|\langle\sigma|\xi\rangle|^2\frac{1}{1+e^{(E_\xi-\mu_T)/k_B\theta}}\ , \quad (3.14)$$

$$\frac{dP_m(t)}{dt}=(\text{gain-loss})_m-\delta_{m,\tau}\left[\frac{P_\tau(t)-P_\tau^{\rm th}}{\tau_\tau}\right]+\delta_{m,\sigma}\left[\frac{P_\sigma^{\rm th}-P_\sigma(t)}{\tau_\sigma}\right]\ , \quad (3.15)$$

$$I(t)=en_e\sum_\tau\frac{P_\tau(t)-P_\tau^{\rm th}}{\tau_\tau}=-en_e\sum_\sigma\frac{P_\sigma(t)-P_\sigma^{\rm th}}{\tau_\sigma}\ . \quad (3.16)$$

We stress that the only states at the tip that contribute to the current (3.16) have a population $P_\tau(t)$ different from the quasiequilibrium $P_\tau^{\rm th}$. In particular, in the low-voltage and low-temperature regimes, the states contributing to the current coincide with those having nonzero projected density of states at the Fermi level in the closed system. If we replace the individual τ's connecting these tip (substrate) states that are relevant to the transport by their average value τ_T (τ_S) and invoke the conservation of the probability inside the STM junction, we reobtain (3.9), where now $P_T=\sum_\tau P_\tau$ and $P_S=\sum_\sigma P_\sigma$ are sums of the respective electron probabilities over the relevant groups of states. It is clear that they are given in the Laplace domain by

$$\tilde P_S(\varepsilon)=\tilde\eta_S(\varepsilon)-\sum_{\tau'}R_{\tau'}\left[\tilde P_{\tau'}(\varepsilon)-\frac{P_{\tau'}^{\rm th}}{\varepsilon}\right]\left[\sum_\sigma\tilde\Pi_{\sigma\tau'}(\varepsilon)\right]-\sum_{\sigma'}R_{\sigma'}\left[\tilde P_{\sigma'}(\varepsilon)-\frac{P_{\sigma'}^{\rm th}}{\varepsilon}\right]\left[\sum_\sigma\tilde\Pi_{\sigma\sigma'}(\varepsilon)\right]\ , \quad (3.17a)$$

$$\tilde P_T(\varepsilon)=\tilde\eta_T(\varepsilon)-\sum_{\tau'}R_{\tau'}\left[\tilde P_{\tau'}(\varepsilon)-\frac{P_{\tau'}^{\rm th}}{\varepsilon}\right]\left[\sum_\tau\tilde\Pi_{\tau\tau'}(\varepsilon)\right]-\sum_{\sigma'}R_{\sigma'}\left[\tilde P_{\sigma'}(\varepsilon)-\frac{P_{\sigma'}^{\rm th}}{\varepsilon}\right]\left[\sum_\tau\tilde\Pi_{\tau\sigma'}(\varepsilon)\right]\ , \quad (3.17b)$$

where the propagators are the Green's functions of Eq. (3.15) in the absence of particle exchanges with the reservoirs.

An averaging approximation, introduced in the context of exciton transport in the presence of multiple traps under the name of the ν-function approximation,[34] will now be used to simplify the analysis considerably. We substitute the sums of the propagators inside the square brackets in (3.17) by their averages. Thus, for example,

$$\Pi_{TT}(t)=\frac{1}{n_T}\sum_{\tau'}\sum_\tau\Pi_{\tau\tau'}(t)w_{\tau'}\ , \quad (3.18a)$$

$$\Pi_{TS}(t)=\frac{1}{n_S}\sum_\sigma\sum_\tau\Pi_{\tau\sigma}(t)w_\sigma\ , \quad (3.18b)$$

and similarly for the other propagators. Here w's are weight factors satisfying $n_S=\sum_\sigma w_\sigma$ and $n_T=\sum_\tau w_\tau$. The substitution of (3.18) into (3.17a) provides directly the Laplace transformed tip population $\tilde P_T(\varepsilon)$ in terms of the difference between the average propagators, the tip population in the closed system $\tilde\eta_T(\varepsilon)$, and the tip quasiequilibrium population $P_T^{\rm th}$. The central result (3.10) of Sec. III A above then follows with the understanding that the Π's are propagator averages as described in (3.18). This

constitutes a usable generalization of Sec. III A.

The integrals of the propagators in our various expressions play the role of inverse effective rates between the electrodes. However, being obtained from microscopic propagators instead of macroscopic rates, they can describe coherence effects in the STM current. Further simplifications of the results can be made by using the relation

$$\eta_T^{\rm th}-P_T^{\rm th}=\frac{1}{n_e}\sum_\tau\sum_m|\langle\tau|m\rangle|^2\left[\frac{1}{1+e^{(E_m-\mu)/k_B\theta}}-\frac{1}{1+e^{(E_m-\mu_T)/k_B\theta}}\right], \tag{3.19}$$

where μ is the chemical potential in the absence of a driving agency. Given the fact that for all normal situations the temperature θ is small compared to the Fermi temperature of the system, we can approximate the Fermi functions in (3.19) and write

$$\eta_T^{\rm th}-P_T^{\rm th}\approx\frac{1}{n_e}\int_{\mu_T}^{\mu}dE\,G_T(E)\ . \tag{3.20}$$

Here $G_T(E)$ is the projected tip density of states at energy E:

$$G_T(E)=\sum_\tau\sum_m|\langle\tau|m\rangle|^2\delta(E_m-E)\ . \tag{3.21}$$

The low-voltage (but arbitrary temperature) expansion $\eta_T^{\rm th}-P_T^{\rm th}\approx(\partial\eta_T^{\rm th}/\partial\mu)_\theta(\mu-\mu_T)$ and the corresponding relation for the substrate yield the Ohmic limit, i.e., Eq. (2.4). In the combined low-voltage low-temperature limit, we further obtain (2.5) in terms of G_T^0 and G_S^0, the projected densities of states evaluated at the Fermi energy E_F. The resistance diverges to infinity when either the tip or the substrate has a zero projected density of states at the Fermi level.

IV. EXPLICIT CALCULATIONS FOR SIMPLE SYSTEMS

We apply the general theory developed above to some specific model situations to illustrate the procedure for the calculation of propagator integrals and to examine the manner in which microscopic factors affect the spatial variation of the current. The first system we study is a chain model with incoherent interactions. Our purpose is to elucidate the effect of the partitioning of the system into the bath and the STM junction. The second system we consider is also a chain model, but with arbitrary degree of coherence. Coherence effects on the *spatial* dependence of the STM current are our target of study in this second system. The third study concentrates on small systems, collections of two, three, and four atoms, also with an arbitrary degree of coherence.

A. Chain models: System-bath partitioning

The study of chain models in the STM context has been shown to be important by García and García,[35] who used numerical solutions of the Schrödinger equation to address long-distance transfer in *thick* adsorbates such as Langmuir-Blodgett films, polyalkanes, proteins, and DNA. The importance of the models arises from the fact that a tunneling mechanism between the tip and the substrate across a 20–50-Å-wide gap is difficult to understand[36,37] in the absence of real transfer to states located in the intervening space. Let us consider our STM junction to be a linear chain of $M+1$ equivalent sites, whose ends are connected to longer chains that represent the bath, the tip being taken as the $(N/2)$th site (N even) and the substrate as the $(N/2+M)$th site. If the evolution of the electron among these sites is incoherent and proceeds via nearest-neighbor rates F, we have

$$\frac{dP_n(t)}{dt}=F[P_{n+1}(t)+P_{n-1}(t)-2P_n(t)]-(F-f)\left[\sum_{k=N/2}^{N/2+M-1}\delta_{k,n+1}P_{n+1}(t)+\sum_{k=N/2-1}^{N/2+M}\delta_{k,n-1}P_{n-1}(t)-2\sum_{k=N/2}^{N/2+M}\delta_{k,n}P_n(t)\right], \tag{4.1}$$

where $P_n(t)$ is the population of the site n at time t. Two features characterize the bath: the ratio M/N, the relative size of the system with respect to the bath size, and the ratio f/F, the inhomogeneity of the junction with respect to the bath. We study first the size effect alone setting $f=F$ and then the inhomogeneity effect using $N/M\to\infty$. For the former case, the propagators are given in the Laplace domain[38] by

$$\tilde{\Pi}_{mn}(\varepsilon)=\frac{\cosh[(N-2|m-n|)\xi/2]}{2F\sinh(\xi)\sinh(N\xi)}\ , \tag{4.2}$$

$$\tilde{\Pi}_{mn}(\varepsilon)=\frac{\cosh[(2N-|m+n-1|-|m-n|)\xi/2]\cosh[(m+n-1|-|m-n|)\xi/2]}{F\sinh(\xi)\sinh(N\xi)}\ , \tag{4.3}$$

where the two results hold for periodic boundary conditions and a chain with ends, respectively, and where ξ is a function of the Laplace parameter ε defined as

$$\cosh\xi=1+\frac{\varepsilon}{2F}\ . \tag{4.4}$$

Since, for the chain under consideration, T and S in (3.6) are the sites $N/2$ and $N/2+M$, respectively, we obtain

$$\tilde{\Pi}_{TT}(\varepsilon)-\tilde{\Pi}_{TS}(\varepsilon)=\frac{\cosh(N\xi/2)-\cosh[(N-2M)\xi/2]}{2F\sinh(\xi)\sinh(N\xi)}\ , \tag{4.5}$$

$$\tilde{\Pi}_{TT}(\varepsilon)-\tilde{\Pi}_{TS}(\varepsilon)$$
$$=\frac{1}{F}\frac{\cosh[(N-1)\xi/2]}{\sin(\xi)\sin(N\xi)}$$
$$\times\{\cosh[(N-2M+1)\xi/2]-\cosh[(N+1)\xi/2]\} \tag{4.6}$$

for the two cases. The effective resistance in the periodic case is thus

$$R_{\text{eff}}=\text{const}[\tilde{\Pi}_{TT}(0)-\tilde{\Pi}_{TS}(0)]$$
$$=\text{const}[\tilde{\Pi}_{SS}(0)-\tilde{\Pi}_{ST}(0)]$$
$$=\text{const}\frac{M}{2F}\left[1+\frac{M}{N}\right], \tag{4.7}$$

while, for the chain with open ends, it is

$$R_{\text{eff}}=\text{const}\frac{M}{2F}\left[1-\frac{M-1}{N}\right]. \tag{4.8}$$

We do not display the constant factor in (4.7) and (4.8) explicitly here. If the number of sites N of the whole chain (STM segment plus bath) is much larger than the number of sites M of the segment, the second contribution in (4.7) and (4.8) is negligible. The bath behaves ideally when $N/M\rightarrow\infty$, i.e., when the number of degrees of freedom of the bath is much larger than the number of degrees of freedom of the system. The effective resistance of the chain segment is that of M resistors in series, each resistor being associated with the resistance $1/2F$. We see here an explicit demonstration of how one might neglect the reservoir rates R appearing in (3.5) and calculate STM quantities only from the junction properties. In the present case, the reservoir rates vanish comfortably in the limit $N/M\rightarrow\infty$.

We next study the case of a STM junction with *unequal rates* ($f\neq F$), embedded in a chain (bath) with rates F, and with $N\rightarrow\infty$ and $M=1$ for simplicity. The evolution (4.1) is readily solved by the defect technique,[39,40] with the help of the translationally invariant Green's functions $\Psi_{mn}=\Psi_{m-n}$ of the periodic system ($f=F$). The propagators are simply related to modified Bessel functions in the time domain

$$\tilde{\Psi}_0(\varepsilon)=\frac{1}{\sqrt{\varepsilon(\varepsilon+4F)}}, \tag{4.9a}$$

$$\tilde{\Psi}_1(\varepsilon)=\frac{2F}{\sqrt{\varepsilon(\varepsilon+4F)}}[\varepsilon+2F+\sqrt{\varepsilon(\varepsilon+4F)}]^{-1}. \tag{4.9b}$$

These, when substituted into the propagator difference

$$\tilde{P}_0(\varepsilon)-\tilde{P}_1(\varepsilon)=\tilde{\Pi}_{TT}(\varepsilon)-\tilde{\Pi}_{TS}(\varepsilon)$$
$$=\frac{\tilde{\Psi}_0(\varepsilon)-\tilde{\Psi}_1(\varepsilon)}{1-2(F-f)[\tilde{\Psi}_0(\varepsilon)-\tilde{\Psi}_1(\varepsilon)]}, \tag{4.10}$$

yield the effective resistance as being proportional to $\tilde{\Pi}_{TT}(0)-\tilde{\Pi}_{TS}(0)=(1/2f)$. This result, while obvious, shows the explicit manner of operation of our expressions and confirms that, in the presence of a reservoir with an infinite number of degrees of freedom, the effective resistance depends entirely on the transport across the STM junction.

B. Chain models: Coherence effects

Coherence effects on the STM current from one of the points of focus of the present paper. Let us consider such effects for the case of an infinite chain. The STM junction consists now of $M+1$ equivalent sites, with longer chains forming the bath as in the first of the models analyzed in Sec. IV A, with N being infinite and the 0th and the Mth site being the tip and substrate, respectively. The evolution equation for the density-matrix elements ρ_{mn} is

$$\frac{d(\rho_{mn}(t)-\rho_{mn}^{\text{th}})}{dt}=-i[H,\rho(t)-\rho^{\text{th}}]_{mn}$$
$$-(1-\delta_{mn})\alpha(\rho_{mn}(t)-\rho_{mn}^{\text{th}}), \tag{4.11}$$

where H is the Hamiltonian and ρ_{mn}^{th} are the thermalized values of ρ_{mn}. Termed the stochastic Liouville equation in exciton dynamics,[32] this equation describes bath interactions through a single dephasing rate α. The Hamiltonian H is simple: electron transfer proceeds via nearest-neighbor interaction matrix elements V. Motion is coherent if $V/\alpha>1$, which would be representative of an electron mean free path much larger than the site-to-site distance in the chain, incoherent if $V/\alpha<1$, which would mean that the electron loses phase memory at every site, and possessing intermediate coherence otherwise. The general procedure[32,40] of using an equation such as (4.11) for STM calculations will be detailed elsewhere.[41] In the context of a theory of transient grating experiments [42], Kenkre has derived an expression for the propagators of (4.11), along with their coherent and incoherent limits. Expressions in the time domain are also available in terms of Bessel functions.[43] The results of Ref. 42 yield, for the present problem,

$$\tilde{\Pi}_{TT}(0)-\tilde{\Pi}_{TS}(0)=\tilde{\Pi}_{SS}(0)-\tilde{\Pi}_{ST}(0)$$
$$=\frac{4}{\pi\alpha}\int_0^{\pi}dk\frac{\sin^2(Mk)}{\sqrt{1+(4V/\alpha)^2\sin^2k}-1}. \tag{4.12}$$

Proceedings as in Ref. 42, it is straightforward to show that (4.12) reduces to a quantity that is proportional to α/V^2 in the incoherent limit and to V in the coherent limit.[44] Using (3.9) and suppressing the explicit factor involving the chemical potential and the electronic charge, we find the dimensionless effective resistance $R_{\text{eff}}^{*}=V\int_0^{\infty}[\Pi_{TT}+\Pi_{SS}-\Pi_{TS}-\Pi_{ST}](t)dt$ to be given in the two extreme limits by

$$R_{\text{incoherent}}^{*}=\frac{1}{2\pi}\left[\frac{\alpha}{V}\right]\int_0^{\pi}dk\left[\frac{\sin(Mk)}{\sin k}\right]^2, \tag{4.13a}$$

$$R_{\text{coherent}}^{*}=\frac{1}{\pi}\int_0^{\pi}dk\frac{\sin^2(Mk)}{\sin k}. \tag{4.13b}$$

A lot of coherence analysis that has been published in the context of exciton transport[32,40] can be brought over into

the STM field through these connections. Experimental I-z characteristics, i.e., curves of current vs tip-substrate separation, exhibit, in the range of large separation, a decay of the current with a rate of one order of magnitude per angstrom. This spatial variation of the current is often used as a rule of thumb in STM to estimate the expected corrugation in the image due to topographic features. The I-z characteristics acquired over the whole range of accessible separations and the observation of anomalous giant corrugation in images of low-index surfaces of metals suggest that the variation of the current with the tip-substrate separation could be slower than in the tunneling regime. The constant-current mode becomes then more sensitive to variations of the current at different scanning locations.

Also of significance in the STM context is the M dependence of the effective resistance as given by (4.12). Figures 1(a) and 1(b) make this dependence clear. It is straightforward to evaluate (4.13a) and show that the spatial dependence in the incoherent limit is linear, i.e., that the effective resistance is proportional to M. One can see from Fig. 1(b) that, in the coherent limit, the spatial dependence (4.13b) is *sublinear*. It can be shown through an analytic procedure[45] that, to an excellent approximation, the dependence in the coherent limit is logarithmic, specifically, that the right-hand side of (4.13b) tends to $(1/\pi)\ln(cM)$, where $c=7.1243$ for large M.

The results of this model indicate two striking consequences of coherence in the STM: a slower decay length with the gap separation and a sublinear dependence of the resistance with the number of sites. Both these effects can change significantly the long-range character of the current relative to predictions of incoherent descriptions.

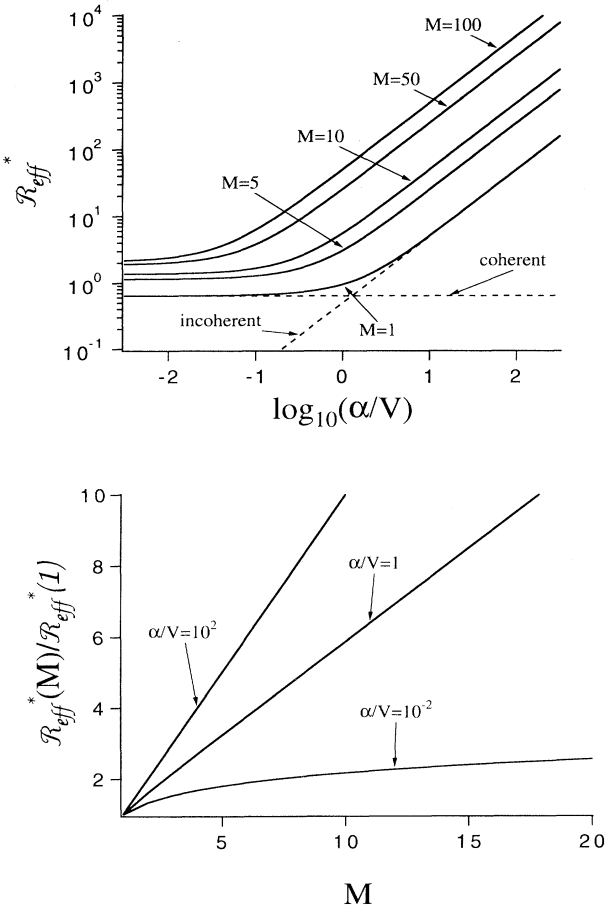

FIG. 1. Coherence effects on the effective STM resistance of a chain segment as given by (4.12) as reflected on the dependence on (a) coherence and (b) length. (a) The dependence on the dephasing rate α for various values of M. Dashed lines are the coherent and incoherent asymptotes from (4.13). (b) The dependence on the length M for different values of α. The resistance is normalized by its value at $M=1$. Notice the sublinear dependence on M in the coherent and partially incoherent regimes.

C. Small systems with arbitrary coherence

We now consider *small* models of the STM junction consisting of a single state T for the tip, a single state S for the substrate, and a small number of states representing the adsorbed molecule. We exclude the singular case $\alpha=0$, but consider otherwise arbitrary degree of coherence. The evaluation procedure consists of calculating the coherent memory functions from the Hamiltonian of the system, using a simple prescription for obtaining from them memory functions in the presence of the bath, and then calculating the propagators from the memory functions. The details of the procedure are described elsewhere.[40,41] Here we report only the results. We consider three illustrative small systems: (i) a two-state system representing only the tip and substrate, (ii) a three-state system in which an adsorbed molecule between the tip and substrate is represented by a single state, and (iii) a four-state system in which the adsorbed molecule is represented by a dimer, i.e., by two states.

1. Two-site system: No adsorbed molecule

The propagator integral in (3.9) is $\int_0^\infty dt[\Pi_{TT}(t)-\Pi_{TS}(t)]=\int_0^\infty dt[\Pi_{SS}(t)-\Pi_{ST}(t)]=(F_{ST}+F_{TS})^{-1}$, where the rates F are given[32] from the Laplace transformed memory functions $\tilde{W}_{mn}(\varepsilon)$ via $F_{mn}=\lim_{\varepsilon\to 0}\tilde{W}_{mn}(\varepsilon)$. For the sake of simplicity, we will consider only resonant systems in this section, i.e., take unperturbed energies to be equal. In terms of the Hamiltonian matrix element V_{ST} between the tip and the substrate and the bath incoherence parameter or dephasing rate α, the effective resistance in (3.9) is given by $R_{\rm eff}=\alpha/2V_{ST}^2$. The analogy between this result and the Fermi golden rule makes clear the well-known fact that $1/\alpha$ plays the role of an effective density of states. The familiar result[15] that the current is proportional to the tip-substrate rate follows directly from the above expression for the propagator integral.

2. Three-site system: A single-state adsorbed molecule

The state representing the adsorbed molecule is labeled by M. The propagator integrals are

$$\int_0^{+\infty} dt[\Pi_{TT}(t)-\Pi_{TS}(t)] = \frac{F_{MS}+2F_{MT}}{3(F_{ST}F_{MS}+F_{ST}F_{MT}+F_{MT}F_{MS})} , \quad (4.14a)$$

$$\int_0^{+\infty} dt[\Pi_{SS}(t)-\Pi_{ST}(t)] = \frac{2F_{MS}+F_{MT}}{3(F_{ST}F_{MS}+F_{ST}F_{MT}+F_{MT}F_{MS})} . \quad (4.14b)$$

We see from (4.14) explicitly the obvious fact that, even if the direct rate F_{ST} connecting the electrodes is negligible, there will be a current if F_{MS} and F_{MT} are nonzero. The M state could generally represent an adsorbate on the substrate, an atom at the tip apex, or a water molecule between the tip and the substrate. Such situations have been modeled by other authors[36,37] in the study of long-distance electron transfer in STM imaging of adsorbates.

To illustrate the usefulness of our theoretical description with emphasis on coherence, we display a result that appears unexpected but is a consequence of the interplay of coherence and transfer. From the counterpart of (4.11) applicable to our present three-state system we can calculate the rates in (4.14) by following an analytic prescription based on projection techniques.[40] The rates are given by

$$F_{ST}=\frac{2\{V_{ST}^4+V_{SM}^2V_{TM}^2+V_{ST}^2[\alpha^2-(V_{SM}^2+V_{TM}^2)]\}}{\alpha[V_{ST}^2+V_{SM}^2+V_{TM}^2+\alpha^2]} , \quad (4.15a)$$

$$F_{MS}=\frac{2\{V_{SM}^4+V_{ST}^2V_{TM}^2+V_{SM}^2[\alpha^2-(V_{ST}^2+V_{TM}^2)]\}}{\alpha[V_{ST}^2+V_{SM}^2+V_{TM}^2+\alpha^2]} , \quad (4.15b)$$

$$F_{MT}=\frac{2\{V_{TM}^4+V_{SM}^2V_{ST}^2+V_{TM}^2[\alpha^2-(V_{ST}^2+V_{SM}^2)]\}}{\alpha[V_{ST}^2+V_{SM}^2+V_{TM}^2+\alpha^2]} . \quad (4.15c)$$

In order to stress the essentials, we now assume that the direct tip-substrate interaction matrix element vanishes. We substitute the resulting form of (4.15) and (4.14), define the quantity $x=(V_{TM}/V_{SM})$, which measures the mismatch of the tip-molecule and substrate-molecule interactions, and denote the constant factor in (3.9) involving the chemical potential and electronic charge by const. We then find the effective resistance to be

$$R_{\text{eff}}=\text{const}\frac{V_{SM}}{2}\left[\frac{\alpha}{V_{SM}}\left[1+\frac{1}{x^2}\right]+\frac{V_{SM}}{\alpha}\left[x-\frac{1}{x}\right]^2\right] . \quad (4.16)$$

Equation (4.16) is a remarkable result. It predicts the occurrence of a *minimum* in the resistance. This minimum occurs at a value of the interaction mismatch x given by

$$x_{\min}^4=1+\left[\frac{\alpha}{V_{SM}}\right]^2 . \quad (4.17)$$

Figure 2, in which we plot the STM current [as the reciprocal of (4.16) in arbitrary units] as a function of $1/x$ for different values of the bath parameter α, makes this quite clear.

As we move the STM tip, the change of its distance from the molecule will be reflected in changes of x. Equations (4.16) and Fig. 2 show that there exits a tip-molecule distance for which the current is a maximum and that this distance is a function of the bath parameter. In the fully coherent case, i.e., when $\alpha=0$, the minimum occurs at the symmetrical configuration, i.e., for $V_{TM}=V_{SM}$. This is a coherence effect arising from quantum-mechanical interference. The symmetrical configuration corresponds to constructive interference. The source of the resistance minimum we predict is precisely the same as that of the Bloch theorem in solid-state physics,[46] which states that a fully periodic lattice does not scatter a current-carrying Bloch state. Departures of one of the lattice constants from the value characteristic of a fully periodic lattice in *either direction* introduce resistance to electron motion.

The second term within the square brackets in (4.16) controls the entire effective resistance in the coherent limit $\alpha=0$, while the first term dominates in the opposite incoherent limit of large α. As the mismatch ratio x increases, equivalently as the distance of the tip from the adsorbate-substrate increases, the incoherent term decreases monotonically and corresponds to the expected variation of the STM current with tip movement. However, the coherent term is *nonmonotonic:* it goes through a minimum and, for tip distances smaller than the characteristic value, it increases as the tip distance de-

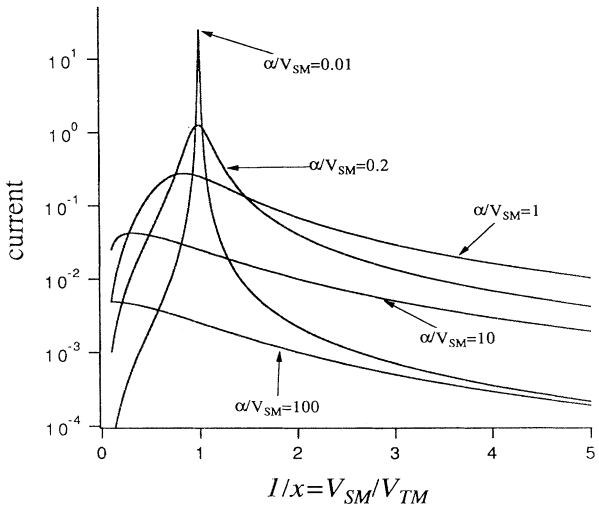

FIG. 2. Quantum interference effects in the STM current showing a nonmonotonic dependence on the tip distance and the occurrence of a maximum in the current. The STM current (in arbitrary units) for a resonant linear three-site system as given by (4.16) is plotted as a function of $1/x=V_{SM}/V_{TM}$ for various degrees of coherence. The abscissa represents the asymmetry of the V's arising from moving the tip, $x=1$ represents the symmetrical configuration, and large values of the abscissa represent large distances of the tip from the molecule-substrate system.

creases. The negative sign in the coherent term apparent in (4.16) signals this interference effect. Figure 3(a) makes clear this expected behavior of the incoherent term and the notable behavior of the coherent term. Viewed from a different perspective, the incoherent term in (4.16) may be called the symmetric term since, in the case $V_{TM}=V_{SM}$, it determines the entire resistance. As Fig. 3(b) shows, this incoherent or symmetric term increases monotonically with the dephasing rate α, whereas the coherent or asymmetric term decreases, with the consequence that, except in the symmetrical configuration $x=1$, where it increases with α, the effective resistance exhibits a minimum with respect to the degree of coherence. We note in passing that Eqs. (4.15) and (4.16) appear to be singular in the coherent limit $\alpha=0$. This is not a practical limitation, but is related to the well-known fact that all Fermi golden rule expressions also break down whenever the energy levels involved are infinitely sharp since the density of states is then pathological. In a similar manner, (4.15) and (4.16) also need modification in the coherent limit $\alpha=0$. Because infinitely sharp levels do not exist in a realistic system, we do not show the modification here. It should be remembered in this context that the reciprocal of α measures the density of states.

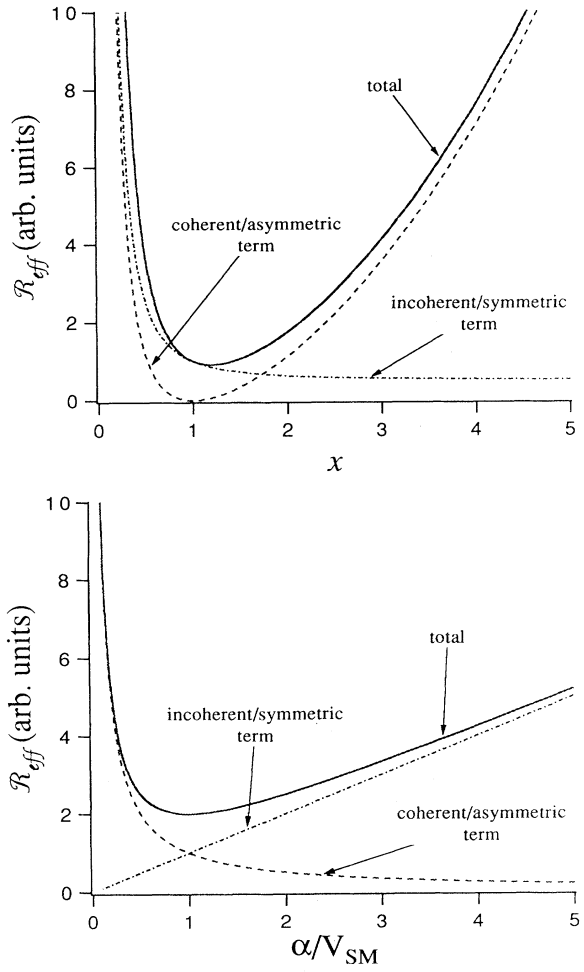

FIG. 3. Interplay of the coherent or asymmetric term (dashed line) and the incoherent or symmetric term (dash-dotted line) in (4.16), which combine to produce the total effective resistance (solid line) with its minimum. (a) The dependence of the effective resistance (in arbitrary units) on the configurational variable $x=V_{TM}/V_{SM}$ for $\alpha/V_{SM}=1$. (b) The dependence on the dephasing rate for $V_{TM}/V_{SM}=1/\sqrt{3}$.

Despite its simplicity, the resonant three-site system we have analyzed in this section has relevance to experiments that have already been conducted. One of them involves imaging of Pt adatoms on a Pt surface with a Pt/Ir tip.[47] Another is the contact resistance experiment,[21] where a sudden increase of the current occurs at short tip-substrate separations. Our prediction is also relevant to the proposal[36] that pressure-induced resonant tunneling through a molecular orbital could be a possible explanation for conduction through thick adsorbed molecules. An extension of the present analysis wherein we relax the resonance condition and address some of these issues will appear elsewhere.

3. *Four-site system: An adsorbed dimer molecule*

Let us now examine the case of an adsorbate with more than one localized orbital between tip and substrate. Such models are caricatures of systems such as CO on Pt,[47] liquid crystals with an aromatic unit and an alkyl chain,[5] dimers of Xe,[48] or Sb (Ref. 49) atoms. We label the molecular states M_1 and M_2 and, as assumed in Secs. IV C 1 and IV C 2, take the direct transfer interaction between the tip and the substrate to be negligible. Three different ways of arranging the dimer with respect to the substrate are studied (Fig. 4): a linear four-site system in which the tip and the substrate are each connected to a single molecular state, a four-site ring in which both molecular states are connected on the tip and the substrate and the molecular states are also interconnected, and the latter system with no interconnections between the two molecular states. We denote these systems respectively by the terms linear, ring, and polygon. As stated above, all sites are taken to be resonant for simplicity.

The intermediate stages of calculation are already quite

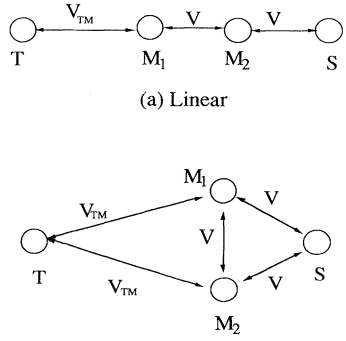

FIG. 4. Resonant four-site models: (a) linear and (b) ring. The third model considered in the text (Sec. IV C), viz., the polygon, is obtained by removing the interaction matrix element between M_1 and M_2 in the ring.

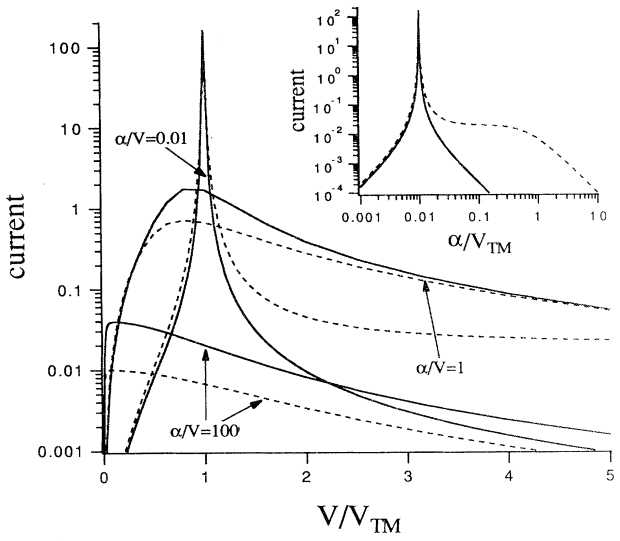

FIG. 5. Dependence of the STM current (in arbitrary units) for the resonant four-site system, vs the configurational variable, at different values of the degree of coherence: ring (solid line) and linear (dashed line). The inset shows the presence of a plateau in the coherent regime ($\alpha/V=0.01$) for the linear tetramer (dashed line), as opposed to the ring (solid line).

involved for this system and will not be shown here. The results are displayed in Fig. 5, where the current is shown as a function of the tip-molecule interaction (representative of the tip distance) for several values of the coherence parameter. The solid line refers to the ring and the dotted line to the linear model. In this scale, the polygon curve coincides with the ring curve.

The qualitative features of the ring are similar to those of the resonant three-site system in Fig. 2, as a consequence of the fact that the bonding eigenstate in the molecule-substrate trimer assists the tunneling. On the other hand, the linear four-site system exhibits a plateau in the current under coherent conditions ($\alpha/V_{SM}=0.01$). The plateau marks a transition region between coherent and incoherent tunneling, characterized respectively by the sharp resonance peak and the monotonic increase in the current [inset in Fig. 5(b)]. As the tip approaches the sample, the plateau appears when $\alpha/V_{TM}\sim 1$ and it bends upward just before reaching the symmetrical configuration. The plateau indicates a region with negligible apparent barrier height and, according to Ref. 22, would be the outcome of a propagation channel connecting the two reservoirs. In terms of our model, the reason lies in the balance between different contributions arising from interference. A detailed analysis of this model will be presented elsewhere.

V. STM IMAGES FOR SIMPLE ILLUSTRATIVE MODELS

The focus of this section, and of the following paper in this series,[41] is the construction of explicit images as predicted by our theory. Detailed images in realistic situations will be given in Ref. 41. Here we study simple two-dimensional models to investigate separately the factors that determine lateral resolution and nontopographical features.

The model for the tip we consider consists of a single site, the substrate consists of ten sites over a length of 20 Å, and the boundary conditions are taken to be periodic in the direction of the extension of the substrate. A tight-binding Hamiltonian with matrix elements

$$H_{mm}=E_m$$
$$H_{mn}=U_{mn}\exp(-\kappa R_{mn}) \quad \text{for } m\neq n \tag{5.1}$$

is adopted to describe the interactions between the various states. The inverse half-decay length κ is taken to be the same for all state pairs, viz., $\sqrt{2}\phi$, where $\phi=0.1837$ a.u.$=5$ eV and R_{mn} measures the relevant distance: between the tip and the adsorbate molecule or between the molecule and a part of the substrate. The spatial dependence of the matrix element is consistent with the decay observed experimentally of the tunneling current. The interaction matrix element $V=H_{\sigma,\sigma\pm1}$ between substrate states scales the interactions, as well as the effective resistance R^*_{eff} defined in Sec. IV. The tip is assumed to be made of the same material as the substrate, so that $H_{T\sigma}/V=\exp[-\kappa(R_{mn}-d)]$, where d is the substrate lattice distance and $E_T=E_S=0$. The nature of the adsorbate is implemented by assigning the values for E_M/V and the preexponential factors U_{MS}/V and U_{MT}/V. The choice of the dephasing rate $\alpha/V=0.5$ makes the STM current 10^{-3} arbitrary units when the tip is about 5 Å from the surface. We take this value as the set point current for the calculation of the images. The value $\alpha/V=0.5$ would correspond to a regime with mixed coherence, i.e., a situation that is not described adequately either by perturbative or by coherent theories. The temperature of the system is taken as $k_B\theta/V=0.025$. The origin of the laboratory frame is taken at the center of the substrate, x is the scanning coordinate, and z denotes the separation between the tip atom and the line of atoms forming the substrate. The positions of the atoms in the actual configuration have been superimposed to emphasize nontopographical effects in the images.

In terms of the above model, we have studied (i) the effect of variations in the strength of the interaction between the adsorbate and the electrodes, (ii) the sensitivity of the STM current to the chemical heterogeneity of the adsorbate, (iii) the lateral resolution in molecular adsorbates and the discrimination of different orientations of the adsorbate, (iv) the effect of the energy mismatch between the molecular state and the Fermi level of the electrodes, and (v) the effect of bath interactions. Our results concerning (i) and (ii), which we have reported earlier,[30] suggest that chemical heterogeneity manifests itself in nontopographical features. This result appears to agree qualitatively with observed images of n-alkyl-p-cyanobiphenyl molecules adsorbed on graphite[50] and $MoSe_2$,[51] where n-unit aliphatic chains appear to be depressed with respect to the aromatic ring. In addition, the lateral size at the base of the protrusion in our result appears to be between 6 and 10 Å, in agreement with ex-

perimental evidence and *ab initio* calculations.[48]

We describe (iii)–(v) in the following. For our study of (iii), we consider a homodimer adsorbed on the substrate. Figure 6(a) shows the constant-current profile of the dimer lying flat on the substrate (M_1 and M_2 are the two localized orbitals on the molecule). It does not reveal the individual units of the homodimer. Both the symmetry and the lateral dimension are similar to those calculated for a single adatom [cf. with the solid line in Fig. 7(a)].

With our parametrization, a resolution of 2 Å in the adsorbate cannot be achieved because of interference effects between the sites of the dimer. The amount of interference varies for different bonding situations. Interactions between the dimer atoms produces constructive interference in between the sites. This results in a peak at the center of the profile as shown by the solid line in Fig. 6(a). The noninteracting dimer, represented by the dashed line, does not involve such interference: the image reflects the actual topography of the homodimer. The difference in height at the center of the dimer between the two cases is of the order of 0.3 Å. This is potentially within the vertical resolution of the scanning tunneling microscope ($\sim$0.1 Å). In Figs. 6(b) and 6(c) the homodimer is rotated around M_1 [at (−1,2) Å] by an angle of 30° and 90° with respect to the surface, respectively. The only manifestation of the actual orientation of the dimer is the difference in the magnitude of the corrugations. The conductance in the proximity of M_2 appears to be enhanced for both the interacting and the noninteracting dimers. Even though the difference in corrugation is within the resolution of the instrument, it

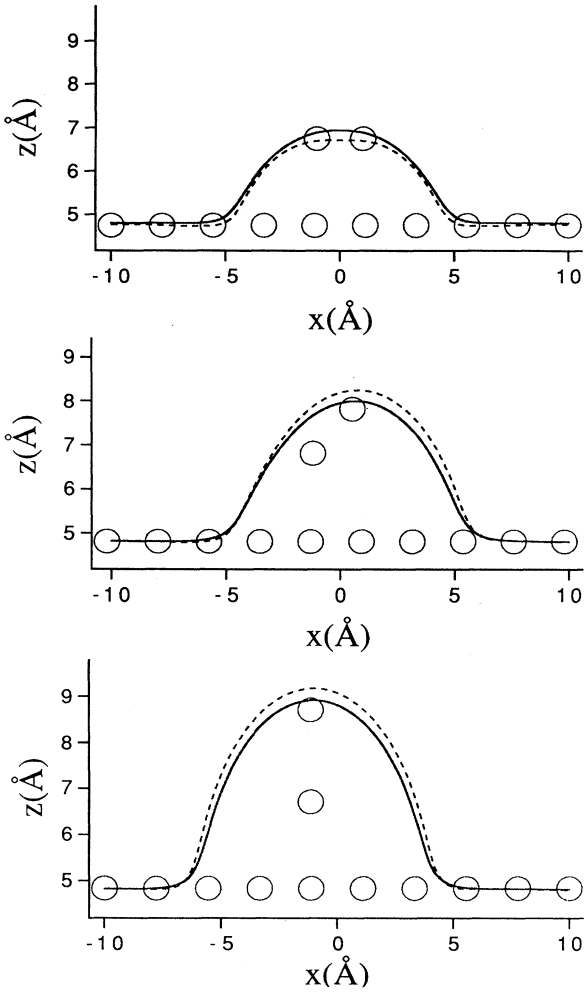

FIG. 6. Sensitivity of the STM image to the molecular orientation and lateral resolution, for a resonant homodimer: (a) flat, (b) tilted 30°, and (c) tilted 90° around M_1 at (−1,2) Å. The substrate plus molecule configuration (shown by circles) is superimposed on the image by matching the substrate with the baseline. The parameters are $U_{M_1M_2}=U_{SS}$ (solid line) and 0 (dashed line). $U_{SM_1}=U_{SM_2}=U_{TM_1}=U_{TM_2}=U_{SS}$. The dimer bond length is 2 Å. The value of α/V is 0.5.

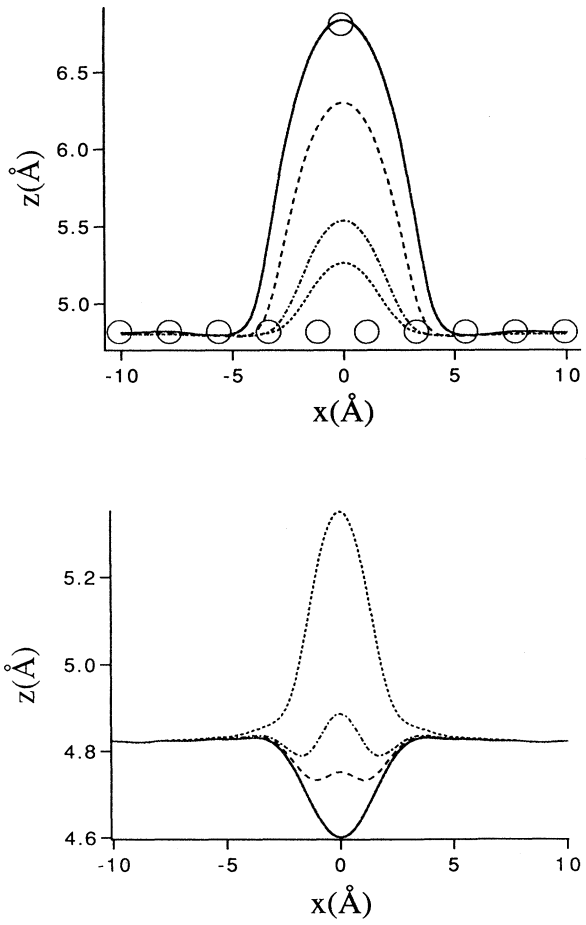

FIG. 7. Dependence of the STM image on the energy mismatch between adsorbate and electrodes for the adsorbate M placed at (0,2) Å. (a) Non-negative-energy mismatch: $E_M/V=0$ (solid line), 1 (dashed line), 5 (dot-dashed line), and 10 (short-dashed line). (b) Negative-energy mismatch $E_M/V=-10$ (solid line), −8.5 (dashed line), −7.5 (dot-dashed line), and −5 (short-dashed line). The parameters are $U_{SM}=U_{TM}=U_{SS}$. The value of α/V is 0.5. The topographical profile in the resonant case is apparent by superimposing the actual configuration (circles) to the base line in (a). All the other cases do not exhibit topographical corrugation.

appears unlikely that the presence of a bond can be inferred from the image when the dimer is tilted.

Figure 7 depicts the result of (iv), i.e., our study of the effects of energy mismatch. An adatom with on-site energy mismatch with respect to the on-site energy of tip and substrate is placed at (0,2) Å. The calculated symmetrical rates F_{mn} are adjusted by multiplicative thermal occupation factors to ensure detailed balance. The images in Fig. 7 do not follow the actual topography, except for the case of the adatom in resonance $E_M=0$. Furthermore, for strong negative-energy mismatch, i.e., when the adatom energy is below the Fermi level of the electrodes, the adatom appears as a negative feature (hole), or with a central depressed protrusion. As the magnitude of the energy mismatch gets smaller, the feature turns positive and it converges with continuity to the resonant case. For positive energy mismatch, the feature is always positive and, as expected, the corrugation decreases as the magnitude of the energy mismatch increases. For extremely large energy mismatches, either positive or negative, the adsorbate becomes transparent. The nature of the nontopographical positive corrugation correlates with the explanation given in the context of the images of Xe on Ni.[48] The latter exhibit a protrusion 1.53 Å high compared to 2.7 Å expected from a hard-sphere model. Holes have been observed experimentally in STM images of O atoms at adsorption sites on Al(111),[52] Ni(100),[53] and Si(111) 7×7 reconstructed surface.[54] In particular, at 300 K O on Ni(100) appears as a hole 0.3 Å in depth and 4 Å in width. For O in Al(111), a central protrusion in the hole at the adsorption site as the tip scans at closer distances has been observed[55] (cf. with the curve for $E_M/V=-8.5$ in Fig. 7). Furthermore, the model exhibits a weak spatial dependence of the corrugation nearby the adatom, as the set point current is decreased, in qualitative agreement with the predictions of Kopatzki and co-workers for O on Al(111).[13]

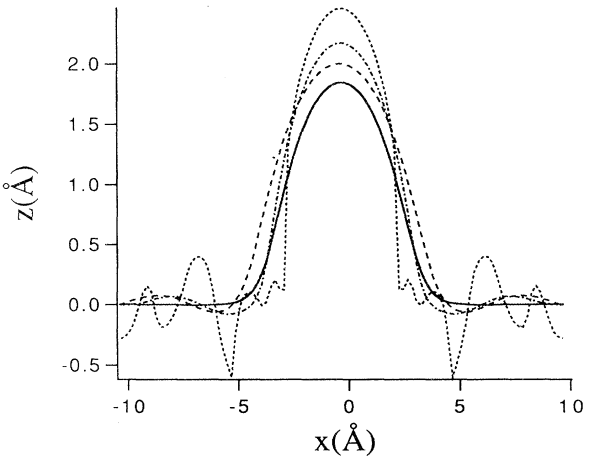

FIG. 8. Dependence of the corrugation in the STM image on the dephasing rate α/V for the resonant adsorbate M placed at (0,2) Å: $\alpha/V=1$ (solid line), 0.5 (dashed line), 0.05 (dot-dashed line), and 0.01 (short-dashed line). The base line of each profile has been aligned to the same zero line to emphasize that the corrugation (peak-to-base line height) increases as the dephasing rate decreases. The oscillations in the tails are symptomatic both of increasing coherence and finite size of the system.

Finally, to study (v), the dephasing rate α/V has been varied, keeping the temperature constant. The trend exhibited in Fig. 8 is that the corrugation increases with the quantum coherence. This is consistent with the deductions we have made in the context of the chain models discussed in Sec. IV.

VI. DISCUSSION

The theoretical framework for the interpretation of STM images presented in this paper has been aimed at a description of images of adsorbates but has wider applicability within STM. Its focus is on a description of STM that accounts for arbitrary magnitude of dephasing reservoir interactions. The latter determine the degree of coherence in electron transfer responsible for quantum interference effects. Our method consists of applying procedures borrowed from quantum statistical mechanics to transfer processes occurring in the STM junction considered as a system of three groups of states, the substrate, the adsorbate, and the tip, in contact with a thermal reservoir. Our point of departure is (3.2) and our formal results are (2.1)–(2.5). They include expressions for the effective resistance of the STM junction and for the STM current, both time resolved and steady state. We have analyzed those results in simple contexts explicitly in Secs. IV and V. The analysis has addressed system-reservoir partitioning, a crossover from linear to sublinear character of the dependence of the effective resistance of the STM junction as a function of coherence, counterintuitive interference effects, and the construction of simple images. The images we have calculated have shown effects of sensitivity of the STM current to the chemical heterogeneity of the adsorbate, raised issues concerning the lateral resolution in molecular adsorbates, and the discrimination of different orientations of the adsorbate, and predicted holes and bumps in images which arise from energy mismatch effects.

Simple consequences of our theory have been shown to have relevance to a number of reported experiments. These include observations on adatoms, such as Xe on Ni(110) or O on Al(111), and on organic molecules such as CO, benzene, or n-CB. We have shown how nontopographical features could arise from chemical heterogeneity and how interference effects could prevent resolution of adsorbates. We have also predicted a maximum in the STM current. This maximum occurs during the variation of either the tip distance or the bath interaction, e.g., through temperature changes. We have given a simple explanation of this maximum in terms of quantum interference. Serious modification in the proper interpretation of observed images may be necessary as a result of this effect.

A detailed comparison between our theory and existing formalisms is under way and will be reported elsewhere. However, a few comments concerning a relation of our results to the transfer Hamiltonian theory[15] might be helpful here. By considering incoherent motion in a STM junction consisting of just the tip and substrate, Eq. (2.5)

is easily shown to correspond to the simple expression

$$I = e^2 \phi_{TS} \frac{F_{ST} + F_{TS}}{(1/G_T^0) + (1/G_S^0)} \tag{6.1}$$

for the current, where F_{TS} is the rate of transition from the substrate to the tip and F_{ST} the rate of transition from the tip to the substrate. Adopting the lowest-order weak-coupling approximation[30] to calculate the transition rate, we can rewrite the rate F_{ST} appearing in Eq. (6.1) as

$$F_{ST} = \frac{2\pi}{\hbar G_T} \sum_{\sigma} \sum_{\tau} |V_{\sigma\tau}|^2 \delta(E_\sigma - E_\tau) \delta(E_F - E_\tau) \ . \tag{6.2}$$

A similar expression holds for F_{TS}. By inserting the sum of these expressions into (6.1), we recover the expression for the transfer Hamiltonian current in the low-voltage limit.[10] It is also possible to develop a suggestive analogy between the propagator integrals in (3.6) and the effective resistance from the Landauer theory of current.[56]

Among the assumptions made in our theory are the vanishing of the reservoir rates, which allow a description in terms of junction parameters alone, and the averaging approximation used in Sec. IV to reduce multistate expressions into effective single-state counterparts. A more severe limitation of our analysis is that imposed by the assumption that linear response is adequate in treating the current. The high electric fields that arise as a result of small tip-substrate distances that occur in STM experiments could modify the very nature of the wave functions in the gap. Despite the fact that this appears to be a limitation of essentially *all* existing theories of STM, we hope to address it in future work. It is worthwhile to mention here that linear response is operative in our formalism only in that no modification of the wave functions by the electric fields is accounted for. Our treatment goes beyond the Ohmic regime, as Secs. II and IV show clearly.

Among the advantages of our approach are the ease of description of quantum interference, the potential to treat temperature effects and bath interactions, and the ability, at least in principle, to go beyond perturbative treatments. Although we have reported the theory as focusing attention on adsorbate images, it is equally applicable to STM systems with no adsorbates. We have been careful to develop the theory in close contact with observations. The verifiable predictions we have made, e.g., the STM current maximum, the illustrative examples we have treated in Sec. VI, and the realistic images we have presented in the following paper in this series, furnish examples of this close contact. A more thorough coherence analysis by extending the single-α description, an elucidation of temperature effects, and a discussion of several specific experiments already existing in the literature are among ongoing work that we hope to report in the near future.

ACKNOWLEDGMENTS

We thank D. H. Dunlap, R. García, and A. Gibson for stimulating discussions. One of us (F.B.) acknowledges the University of Oregon–Institute of Molecular Biology for support and the Istituto di Biofisica–CNR, Pisa, Italy for partial support and thanks C. Ascoli and C. Frediani for their encouragement.

*Present address: Istituto di Spettroscopia Molecolare ed Istituto LAMEL Consiglio Nazionale delle Ricerche, Via Gobetti 101, 40129 Bologna, Italy.

[1]G. Binnig, H. Rohrer, C. Gerber, and E. Weibel, Appl. Phys. Lett. **40**, 178 (1982).
[2]V. M. Hallmark, S. Chiang, I. F. Rabolt, J. D. Swalen, and R. J. Wilson, Phys. Rev. Lett. **59**, 2879 (1987).
[3]J. Wintterlin, J. Wiechers, H. Brune, T. Gritsch, H. Höfer, and R. J. Behm, Phys. Rev. Lett. **62**, 59 (1989).
[4]H. Ohtani, R. J. Wilson, S. Chiang, and C. M. Mate, Phys. Rev. Lett. **60**, 2398 (1988); P. H. Lippel, R. J. Wilson, M. D. Miller, C. Wöll, and S. Chiang, *ibid.* **62**, 171 (1989).
[5]J. K. Spong, H. A. Mizes, L. J. LaCombe, Jr., M. M. Dovek, J. E. Frommer, and J. S. Foster, Nature **338**, 137 (1989).
[6]V. M. Hallmark and S. Chiang, Surf. Sci. **286**, 190 (1993).
[7]N. García, C. Ocal, and F. Flores, Phys. Rev. Lett. **50**, 2002 (1983).
[8]E. Stoll, A. Baratoff, A. Selloni, and P. Carnevali, J. Phys. C **17**, 3073 (1984).
[9]A. A. Lucas, H. Morawitz, G. R. Henry, J.-P. Vigneron, P. Lambin, P. H. Cutler, and T. E. Feutchwang, Phys. Rev. B **37**, 10 708 (1988).
[10]J. Tersoff and D. R. Hamann, Phys. Rev. Lett. **50**, 1998 (1983).
[11]N. D. Lang, Phys. Rev. Lett. **55**, 230 (1986).
[12]M. Tsukada and N. Shima, J. Phys. Soc. Jpn. **56**, 2875 (1987).
[13]G. Doyen, D. Drakova, E. Kopatzki, and R. J. Behm, J. Vac. Sci. Technol. A **6**, 327 (1988); E. Kopatzki, G. Doyen, D. Drakova, and R. J. Behm, J. Microsc. **152**, 687 (1988).
[14]N. D. Lang, Phys. Rev. Lett. **56**, 1164 (1986).
[15]J. Bardeen, Phys. Rev. Lett. **6**, 57 (1961).
[16]J. Tersoff and D. R. Hamann, Phys. Rev. B **31**, 805 (1985).
[17]A. Selloni, P. Carnevali, E. Tosatti, and C. D. Chen, Phys. Rev. B **31**, 2602 (1985).
[18]R. M. Tromp, R. J. Hamers, and J. E. Demuth, Phys. Rev. B **34**, 1388 (1986).
[19]C. J. Chen, Phys. Rev. Lett. **65**, 448 (1990).
[20]W. Sacks and C. Noguera, Phys. Rev. B **43**, 11 612 (1991).
[21]J. K. Gimgewski and R. Möller, Phys. Rev. B **36**, 1284 (1987).
[22]N. D. Lang, Phys. Rev. B **36**, 8173 (1987).
[23]M. Tsukada, K. Kobayashi, N. Isshiki, and H. Kageshima, Surf. Sci. Rep. **13**, 265 (1991).
[24]G. Doyen, E. Koetter, J. P. Vigneron, and M. Scheffler, Appl. Phys. A **51**, 281 (1990).
[25]C. Noguera, Phys. Rev. B **42**, 1629 (1990).
[26]C. J. Chen, Phys. Rev. B **42**, 8841 (1990).
[27]P. Sautet and C. Joachim, Chem. Phys. Lett. **185**, 23 (1991).
[28]T. N. Todorov and A. P. Sutton, Phys. Rev. Lett. **70**, 2138 (1993).
[29]J. B. Pendry, A. B. Prêtre, and B. C. H. Kreutzen, J. Phys. Condens. Matter **3**, 4313 (1991).
[30]V. M. Kenkre, F. Biscarini, and C. Bustamante, Ultramicroscopy **42-44**, 111 (1992).

[31]R. Silbey, Annu. Rev. Phys. Chem. **27**, 203 (1976).
[32]V. M. Kenkre and P. Reineker, in *Exciton Dynamics in Molecular Crystals and Aggregates,* edited by G. Hohler, Springer Tracts in Modern Physics Vol. 94 (Springer-Verlag, Berlin, 1982).
[33]R. Kubo, M. Toda, and N. Hashitsume, *Statistical Physics II: Nonequilibrium Statistical Mechanics* (Springer, Berlin, 1985).
[34]V. M. Kenkre, Chem. Phys. Lett. **93**, 260 (1982); see also V. M. Kenkre and P. E. Parris, Phys. Rev. B **27**, 3221 (1983).
[35]N. García and R. García, Chem. Phys. Lett. **173**, 44 (1990).
[36]S. M. Lindsay, O. F. Sankey, Y. Li, C. Herbst, and A. Rupprecht, J. Am. Chem. Soc. **94**, 4655 (1990).
[37]C. Joachim and P. Sautet, in *Scanning Tunneling Microscopy and Related Methods,* edited by R. J. Behm *et al.* (Kluwer Academic, Dordrecht, 1990), p. 377.
[38]K. Lakatos-Lindenberg, R. P. Hemenger, and R. M Pearlstein, J. Chem. Phys. **56**, 4852 (1972); see also V. M. Kenkre and Y. M. Wong, Phys. Rev. B **23**, 3748 (1981).
[39]E. W. Montroll and B. West, in *Fluctuation Phenomena,* edited by E. W. Montroll and J. B. Lebowitz (North-Holland, Amsterdam, 1979).
[40]V. M. Kenkre, in *Energy Transfer Processes in Condensed Matter,* edited by B. D. Bartolo (Plenum, New York, 1984), p. 1.
[41]F. Biscarini, C. Bustamante, and V. M. Kenkre, following paper, Phys. Rev. B **51**, 11 089 (1995).
[42]V. M. Kenkre, Phys. Rev. B **18**, 4064 (1978).
[43]V. M. Kenkre and S. M. Phatak, Phys. Lett. **100A**, 101 (1984).
[44]V. M. Kenkre and R. S. Knox, Phys. Rev. Lett. **33**, 803 (1974).
[45]D. H. Dunlap (private communication).
[46]N. W. Ashcroft and N. D. Mermin, *Solid State Physics* (Holt, Rinehart and Winston, New York, 1976).
[47]P. Zeppenfeld, C. P. Lutz, and D. M. Eigler, Ultramicroscopy **42-44**, 128 (1992).
[48]D. M. Eigler and E. K. Schweizer, Nature **344**, 524 (1990); D. M. Eigler, P. S. Weiss, E. K. Schweizer, and N. D. Lang, Phys. Rev. Lett. **66**, 1189 (1991).
[49]Y. W. Mo, Science **261**, 886 (1993).
[50]D. P. E. Smith, H. Hörber, C. Gerber, and G. Binnig, Science **245**, 43 (1989).
[51]M. Hara, Y. Iwakabe, K. Tochigi, H. Saasabe, A. F. Garito, and A. Yamada, Nature **344**, 228 (1990).
[52]H. Brune, J. Wintterlin, G. Ertl, and R. J. Behm, Europhys. Lett. **13**, 123 (1990).
[53]E. Kopatzki and R. J. Behm, Surf. Sci. **245**, 255 (1991).
[54]P. Avouris and I.-W. Lyo, Surf. Sci. **242**, 1 (1991).
[55]J. Wintterlin and R. J. Behm, in *Scanning Tunneling Microscopy I,* edited by H.-J. Guntherodt and R. Wiesendager (Springer-Verlag, Berlin, 1992), p. 39.
[56]R. Landauer, Philos. Mag. **21**, 863 (1970).